

OPTIMIZATION OF MONOCLINIC Cu_2SnS_3 (CTS) THIN FILM SOLAR CELL PERFORMANCES THROUGH NUMERICAL ANALYSIS

M. Y. ALI^{a,*}, M. A. ABEDIN^a, M. S. HOSSAIN^a, E. S. HOSSAIN^a

^a*Department of Electrical and Electronic Engineering, Dhaka University of Engineering Technology, Gazipur-1700, Bangladesh*

Investigation on the performance of monoclinic phase copper tin sulfide (CTS) based thin film solar cells has been carried out numerically by AMPS-1D simulation software. Based on proposed cell structure, the influence of carrier concentration and thickness of both absorber and buffer layers as well as the work function of back contact metal are studied to enhance the output performance of monoclinic phase CTS thin film solar cell. The effect of operating temperature is also tested for CTS solar cell to ensure the sustainability at outdoor installation. After optimizing the thickness and carrier concentration of both layers, the best CTS cell is delivers 9.61% efficiency with back contact of molybdenum. However, after optimization of back contact metal work function the conversion efficiency is further increased to 17.87% for tungsten as back contact metal with a work function of 5.25 eV. The increased temperature shows a negative effect on output performance with a decline efficiency rate of -0.33/K. All these simulation results will give some important guides for feasibly fabricating higher efficiency CTS solar cells.

(Received November 29, 2019; Accepted February 20, 2020)

Keywords: Thin film solar cell (TFSCs), Copper tin sulfides (CTS), Work function, Numerical simulation, AMPS-1D

1. Introduction

The need to produce renewable energy with low production cost and high efficiency (Eff) is indispensable in making the dream of avoiding undue reliance on fossil fuel. Though, first generation crystalline silicon based solar cell has shown the highest PCE of 26.7% [1], second generation thin film based solar cells technology has greater advantage in terms of reduced raw material utilization, less manufacturing process and superior performance capability at practical operating condition. Cadmium Telluride (CdTe) and Copper Indium Germanium Sulfides (CIGS) are the two pioneer second generation thin film based solar cell which have presented the highest PCE of 21.0% and 23.4% correspondingly [1]. However, due to the use of toxic (Cd) and rare (Te, In) earth material, they are not suitable for massive level electricity production [2-3]. In the last few decades, kesterite mineral shaped Copper Zinc Tin Sulfides (CZTS) has undergone laborious research as all the consisting elements are earth abundant and eco- friendly as well as it inherits all the necessary photovoltaic properties of the well-established thin film CIGS based solar cell. Having direct bandgap (1~1.5 eV) and p-type conductivity with high absorbance coefficient (10^4 cm^{-1}), CZTS based solar cell has been reported the highest record PCE of 12.6% [4]. However, controlling of simultaneous four elements as well as the formation of secondary phases spot the synthesis of pure kesterite phase CZTS absorber layer really challenging.

The performance in CZTS film is limited by low open circuit voltage (V_{oc}) due to recombination loss with activation energy less than the bulk band gap high series resistance and double diode behavior in the current-voltage characteristics especially in the thicker film [5]. Due

* Corresponding author: sabbir@duet.ac.bd

to this constraint an alternative material CTS with relatively similar earth abundances and non-toxicity is highly sought [6]. Copper Tin Sulfides (CTS) is the one of the prime secondary phase, which has most often seen as a byproduct along with CuS and SnS during the fabrication process of CZTS absorber layer [7]. As a result, enormous interest to explore the properties of the CTS as an absorber layer has been turned on. As a ternary compound, CTS shows similar properties like CZTS having P-type conductivity with very high absorption coefficient (10^5 cm^{-1}) along with optimal bandgap range (0.9 ~ 1.6 eV) [8-11]. As like CZTS, the component materials of CTS are also nontoxic and earth abundant whereas the synthesis process of the later one is easier to control due to having less number of components. More importantly with the absence of Zn in CTS material system, the unfavorable $[\text{Cu}_{\text{Zn}} + \text{Zn}_{\text{Cu}}]$ defect complex can be completely avoided [12]. CTS based solar cell was first fabricated by Kuku and Fakulujo at 1987 showing the PCE of 0.11% [13] and currently the record PCEs for CTS based solar cells are 4.6% (Na doped CTS) [14] and 6% (Ge alloyed CTS-CTGeS) [15], indicating that the progress towards of CTS solar cell is still in its primary stage. Due to lack of octet rule, CTS can be formed in various phases such as hexagonal, cubic, tetragonal, monoclinic, triclinic and orthorhombic are reported so far [11, 16-18]. Among them, monoclinic CTS phase has been reported as the most successful full cell device [8, 19-20]. Recently, a comparison study among the cubic, tetragonal and orthorhombic phases of CTS based solar cell has been reported [6]. However, no simulation study has been yet reported for the monoclinic phase CTS based thin film solar cell (TFSC).

In this study monoclinic phase CTS based TFSC has been studied with the help of numerical simulation. We know that numerical simulation is an efficient way to predict the effect of changes in material properties, assess the potential merits of cell structures and then optimize the structure of cells. It is an important way to predict cell performance and to test the viability of the proposed structure. As such in this work a numerical simulation, based on AMPS-1D (Analysis of Microelectronic and Photonic Structures) is performed to investigate the effect of monoclinic phase CTS absorber layer thickness and carrier density. The effect of buffer layer thickness on the performance of solar cell is also studied. Finally, the effects of different back contact metals on the performance of CTS devices are studied to identify an optimal back contact metal for monoclinic phase of CTS compound. Then the resulting changes in open circuit voltage (V_{oc}), short circuit current density (J_{sc}), fill factor (FF) and Eff are recorded and plotted to assess the performance.

2. Numerical modeling and simulation parameters

Numerical study is an important pre-requisite of solar cell fabrication to assess the influences of various model parameters and optimize them in a cost efficient way. In this work, numerical modeling of CTS based TFSC has been carried out by AMPS-1D (Analysis of microelectronic and Photonic Structures) computer based software, which was developed by Stephen Fonash et al. of Pennsylvania State University in 1999 [21]. AMPS-1D is a one dimensional device level simulation tool, which is capable to replicate the working principle of heterojunction, homojunction, multijunction and even Schottky barrier based solar cell device structures and can be employed by specifying the semiconductor parameters in each defined layer of device structures as input parameters of the simulations. This software has been proven as powerful solar cell simulator tool in understanding the device operation and physics for single crystal, poly-crystal and amorphous structures, which is widely used by numerous research group [22]. Finite differences and Newton Raphson iteration techniques are employed in this program to find out the solution of one dimensional continuity equations and poisson's equation for both electron and hole. With accurate modeling and by incorporating the required materials parameters, this simulator can precisely calculate the output performances and insight device parameters of photovoltaic device such as V_{oc} , J_{sc} , FF, Eff, space charge region distribution, generation and recombination profiles of charge carrier and spectral response [6, 23-24].

Substrate type heterojunction device stack configuration of Al/n-ZnO:Al/i-ZnO/n-CdS/p-CTS/Mo/SLG as shown in Fig. 1 is employed in this work, which has been taken from the well-established and proven technological standard of CIGS and CZTS solar cell [4, 25]. The aforesaid structure consists of soda lime glass (SLG) as a substrate, molybdenum (Mo) as a back contact,

CTS as a p-type absorber layer (p-CTS), cadmium sulfide (CdS) as a n-type buffer layer (n-CdS), intrinsic zinc oxide (i-ZnO) as a highly resistive transparent window (HRT) layer, aluminum doped ZnO (ZnO:Al) as a transparent conducting oxide (TCO) layer and finally Al as a front contact metal layer. The device is considered to be illuminated from the TCO to the end of the device with the AM1.5 spectrum (1 kW/m^2). Accuracy of simulated results directly depends on the relative accurateness of input material parameters of various layer of respective device. Therefore, material parameters of CTS absorber layer are selected precisely from authentic literature, theory and in some cases reasonable assumptions to reflect the possible outcome as practical experimental condition [14].

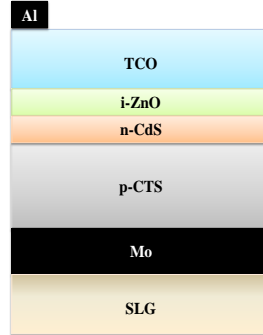


Fig. 1. Substrate type CTS based TFSC device stack configuration.

Table 1. Interfacial contact parameters used in this study.

Interface Parameters	Al/TCO	CTS/back contact
Barrier height ϕ_b (eV)	$\phi_{bn} = 0$	$\phi_{bp} = \sim$
Electron surface recombination velocity, S_e (cm s^{-1})	$1.00\text{e}+7$	$1.00\text{e}+7$
Hole surface recombination velocity, S_h (cm s^{-1})	$1.00\text{e}+7$	$1.00\text{e}+7$

Table 2. Layer parameters used in this study.

Layer Parameters	TCO	i-ZnO	CdS	CTS
Layer thickness (nm)	200	50	20 ~ 80	1000 ~ 4000
Dielectric constant, ϵ_r	9	9	10	10
Electron mobility, μ_n ($\text{cm}^2/\text{V.s}$)	100	100	350	100
Hole mobility, μ_p ($\text{cm}^2/\text{V.s}$)	25	25	25	25
Acceptor concentration, N_A (cm^{-3})	0	0	0	$1.00\text{e}+13 \sim 1.00\text{e}+19$
Donor concentration, N_D (cm^{-3})	$1.00\text{e}+18$	$1.00\text{e}+13$	$1.00\text{e}+13 \sim 1.00\text{e}+19$	0
Band gap, E_G (eV)	3.30	3.30	2.40	0.89
Effective density of states in conduction band, N_C (cm^{-3})	$2.20\text{e}+18$	$2.20\text{e}+18$	$1.80\text{e}+19$	$2.20\text{e}+18$
Effective density of states in valence band, N_V (cm^{-3})	$1.80\text{e}+19$	$1.80\text{e}+19$	$2.40\text{e}+18$	$1.80\text{e}+19$
Electron affinity, χ (eV)	4.6	4.6	4.2	4.77
Gaussian defect density, N_G (cm^{-3})	$1\text{e}+17$	$1\text{e}+17$	$1\text{e}+18$	$1\text{e}+15$

The basic properties of front (Al/TCO) and back (CTS/Mo) interfacial metal-semiconductor contacts applied in this work are recorded in the following Table 1. The front contact was ensured as a standard ohmic contact by assuming flat band scenario (0 eV electron barrier height) between front contact metal Al and TCO, whereas electron barrier height resulted from the band alignment of back metal to CTS junction was subjected to optimize for different

back metal work function Numerical values of TCO, i-ZnO and CdS layers are listed in Table 2, while their optical absorption coefficients were collected from the report done by Gloeckler et al. [27]. Optical absorption coefficients as well as band gap value of monoclinic CTS phase was collected from the experimental study reported by Chalapathy et al. [28], whereas the value of electron affinity was taken from the report done by Avellaneda et al. [16]. All these values of p-CTS layer are also listed in Table 2.

3. Results and discussion

3.1. Effect of absorber layer thickness and carrier concentration

Thickness plays an important role for semiconductor devices especially in thin film where the carrier diffusion length is a constraint. In TFSCs particularly a large part of the entire device's thickness is occupied by the absorber layer which plays the role of the active layer and in which the majority of photons having energy greater than or equal to the band gap energy of the material is absorbed [26]. It is therefore important and essential to control the absorber layer thickness, which cell can be controlled by both deposition time and sulfurization scheme [29]. Moreover,

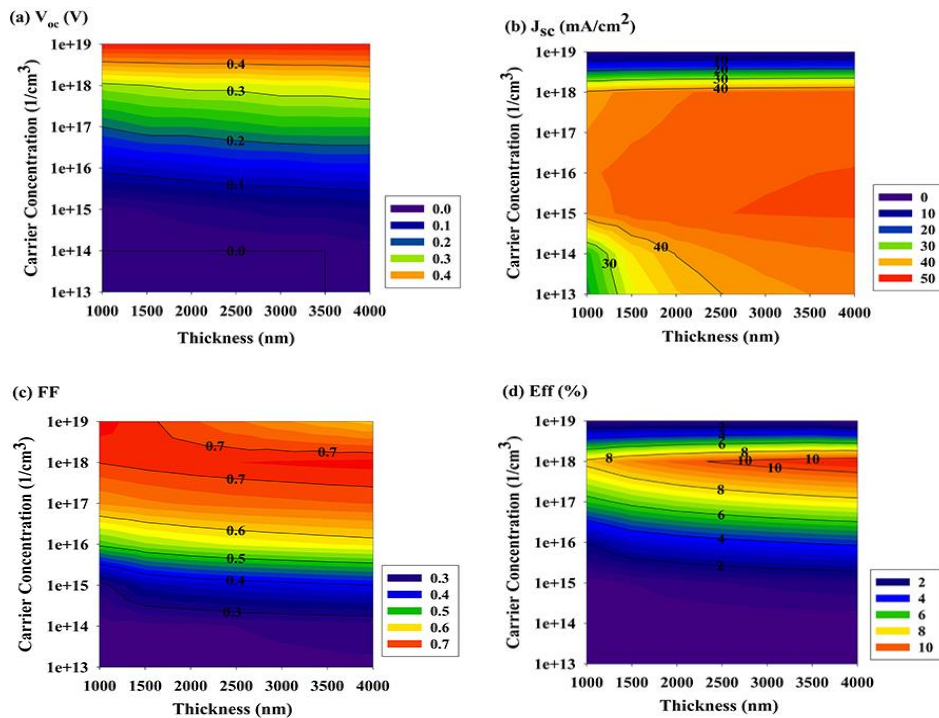


Fig. 2. Concurrent effect of thickness and carrier concentration of absorber layer on the performance of CTS based solar cell.

CTS has been proved as a p-type self-doping semiconductive material, which originates from the stoichiometric discrepancy of Cu/Sn ratio. The desired doping level of CTS semiconductive material can be achieved by controlling the Cu/Sn ratio as well as the sulfurization temperature [30-31]. Copper vacancy sites (V_{Cu}) are mainly responsible for the acceptor type carrier concentration of CTS material. Therefore, copper poor and Sn rich CTS based solar cell has shown desirable photovoltaic properties and higher efficiency [13]. In the following subsections, the performance of the CTS based solar cell is evaluated by the four key output parameters, such as J_{sc} , V_{oc} , FF and Eff. However, in some cases the inward characteristics of CTS absorber layer is analyzed through depletion width, spectral response and electric field strength.

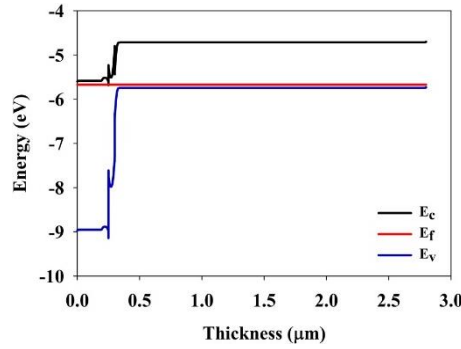


Fig. 3. Energy band diagram of monoclinic CTS phase absorber layer and CdS buffer layer.

Fig. 2(a) depicts the concurrent effect of thickness and carrier concentration of absorber layer on the V_{oc} of monoclinic phase CTS solar cell. Variation of absorber layer thickness does not affect significantly on V_{oc} . This is because the increased thickness helps to trap more photons of longer wavelength which increases the current density as mentioned earlier. However, the increased thickness also introduced an amplified series resistance which limits the V_{oc} . On the other hand, due to acceptor concentration, open circuit voltage changes gradually showing the lowest value for $10^{13}/\text{cm}^3$ and the highest for the concentration at $10^{19}/\text{cm}^3$. According to Eqn. (1) and Eqn. (2) given below, increasing carrier concentration decreases the saturation current which in turns increases the V_{oc} .

$$I_0 = An_i^2 \left(\frac{D_e}{L_e N_A} + \frac{D_h}{L_h N_D} \right) \quad (1)$$

where, A is the cross-sectional area of p-n heterojunction, n_i is the intrinsic carrier concentration, L_e is the diffusion length of electrons in the p-side, L_h is the diffusion length of hole in the n-side, D_e is the diffusion coefficient of electron, D_h is the diffusion coefficient of hole, N_A is the donor concentration, and N_D is the acceptor concentration.

$$V_{oc} = \frac{kT}{q} \ln \left(\frac{I_L}{I_0} + 1 \right) \quad (2)$$

where, T, k, q, I_0 , and I_L are operating temperature Boltzmann constant, electric charge of electron, and reverse saturation current, and photo-generated current, respectively. According to basic photovoltaic theory, a denser medium creates a longer diffusion path. Hence, increasing carrier concentration also raises the diffusion length which also contributes reducing saturation current and thereby increasing the V_{oc} . From general semiconductive theory it can be anticipated that lower band gap generates more photo-generated current while lowering built in potential which in turns declines the V_{oc} . Therefore, monoclinic phase CTS absorber having the bandgap of 0.89 eV displays the V_{oc} of 0.2 eV for the thickness and carrier concentration of 2 μm and $10^{17}/\text{cm}^3$, respectively. For the same thickness and carrier concentration, cubic phase CTS based solar cell having more band gap (0.96 eV) showed more V_{oc} (0.25 V) than this monoclinic phase CTS solar cell [6]. Beside this, the band alignment of absorber/buffer layer is also controls the value of V_{oc} . A spike type band alignment possesses positive conduction band offset (CBO), which generates more built-in potential than cliff-type band alignment (type-II) [31]. In this study, CTS/CdS shows type-II band alignment (Fig. 3) which generates less built-in potential and thus lower V_{oc} .

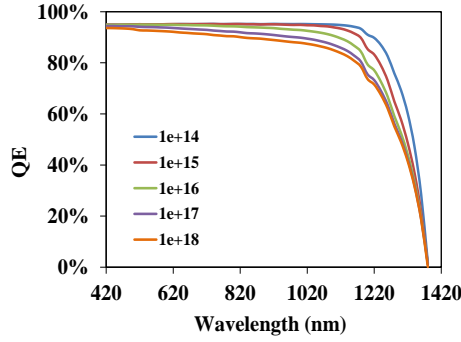


Fig. 4. Effect of acceptor concentration of absorber layer on the QE of CTS based solar cell.

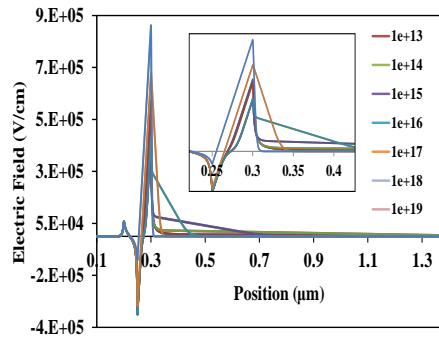


Fig. 5. Effect of acceptor concentration on the electric field of CTS/CdS interface (the critical region has been shown largely inside).

Fig. 2(b) shows the concurrent effect of carrier concentration and thickness of absorber layer on the J_{sc} monoclinic phase CTS based solar cell. According to increasing carrier concentration of p-type absorber layer which is also known as acceptor concentration reduces the lifetime of electrons, which results in decreasing probability of carrier collection and thereby, declines the quantum efficiency (QE), as shown in Fig. 4. However, the effect of carrier concentration of absorber layer mostly noticeable on the depletion width, which is the crucial parameter for determining the photo-generated current density. Fig. 5 shows the width of depletion width of absorber/buffer $p-n$ junction for the monoclinic phase CTS based solar cell. The following Eqn. 3 [33] and Eqn. 4 [34] show the theoretical relation between depletion width (W_d) of $p-n$ junction and the maximum photo-generated current (I_{ph}):

$$W_d = \left[\frac{2\varepsilon_1\varepsilon_2(V_{bi}-V)(N_A^2+N_D^2)}{q(\varepsilon_1N_D+\varepsilon_2N_A)N_DN_A} \right]^{\frac{1}{2}} \quad (3)$$

$$I_{ph} = qAG(L_e + W_d + L_h) \quad (4)$$

where, ε_1 , ε_2 , V_{bi} , V , G are the dielectric permittivity of buffer layer, dielectric permittivity of absorber layer, built-in voltage, applied voltage, generation rate of electron-hole pair, respectively, and the rest of symbols have been described previously for equation 1 and 2. The linear proportional relation between depletion width and photo-generated current described in equation 4 can be clarified by field effect theory, which states that, the effect of field extends to the boundary line of depletion region to attract the photo-generated electron to the buffer layer [6], thus a wider depletion region ensures more photo-generated current. From Fig. 6, it is evident that, the depletion width is increasing up to the carrier concentration of $10^{15}/\text{cm}^3$ and then it declines. The variation acceptor concentration shows the similar effect on J_{sc} which can be seen from Fig. 2 (b) and the highest value of J_{sc} ($> 45 \text{ mA}/\text{cm}^2$) has been found for acceptor concentration of $10^{15}/\text{cm}^3$.

This value then declines a little with increasing acceptor concentration and reaches about 40 mA/cm² for the acceptor concentration of 10¹⁸/cm². However, as the acceptor concentration increases further to 10¹⁹/cm², J_{sc} abruptly changes to lower than 5 mA/cm². This phenomenon can be clarified by the ‘Mott transition’ rule, which describes that, semiconductor material losses its semiconductive properties after a certain doping level and shows metallic behavior [35]. This certain doping level is known as critical doping level, which is calculated as 10¹⁸/cm³ from the following Eqn. (5) [36]:

$$N_{crit} \approx (0.24/a_B^*)^3 \quad (5)$$

whereby, $\epsilon_r \approx 10$, m_e (effective mass of electron) = 0.18× m_0 (rest mass of electron), a_B is the Bohr radius of Hydrogen, and a_B^* (effective Bohr radius) = $a_B(\epsilon_r/m_e)$. The sudden change of J_{sc} can also be explained with the doping level of absorber and buffer layer by ref. [32], which states that, as long as the acceptor concentration of absorber layer remains smaller than donor concentration of buffer layer, the mostly states of interface defects are occupied by electrons. However, as the acceptor concentration of absorber goes beyond the donor concentration of buffer layer, then the interface defects states are mostly occupied by holes, which act as electron traps in the *p-n* junction interface. Severe interface recombination happens due to these electron traps and therefore, electron flow is relentlessly declined from the junction to the front contact of the solar cell. Since, in this work the donor concentration is taken as 10¹⁸/cm², therefore the value of J_{sc} suddenly changed to much lower value as the acceptor concentration of absorber layer is increased beyond the critical of 10¹⁸/cm². On the other hand, thickness of absorber layer has a significantly impact on J_{sc} for the lower acceptor concentration. From the Fig. 2 (b), it can be seen that, up to acceptor concentration of 10¹⁵/cm², the J_{sc} is increased almost linearly with increasing absorber layer thickness. However, as the acceptor concentration exceeds 10¹⁵/cm², the J_{sc} is only slightly varied up to the thickness of 2000 nm, and remain almost constant onward the end. Therefore, a CTS absorber of 2000 nm thickness with a acceptor concentration of 10¹⁸/cm² can be selected as the optimum values from the J_{sc} analysis, which are also experimentally realistic values for CTS based solar cell [30].

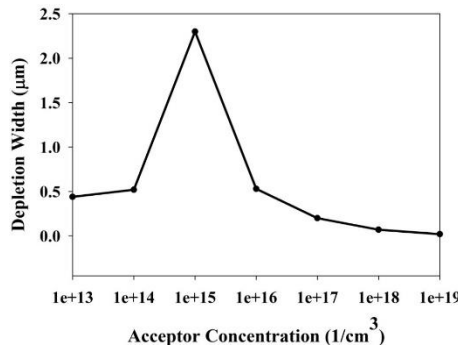


Fig. 6. Variation of the width of depletion region of CTS/CdS interface according to acceptor concentration.

Fig. 2(c) shows the effect of thickness and carrier concentration of absorber layer on the FF of the CTS based solar cell, which is referred as a measurement of “rectangularity” of the V-I curve of solar cell [6]. Ideally, the value of FF can be related to V_{oc} by the Eqn. (6) [37]:

$$FF = \frac{v_{oc} - \ln(v_{oc} + 0.72)}{v_{oc} + 1} \quad (6)$$

where, v_{oc} (normalize voltage) = $V_{oc}/(kT/q)$. In practical condition, this FF also depends on the recombination mechanism in addition with V_{oc} . As can be seen from Fig 2(c), the value of FF is varies from 0.3 to 0.7 as the acceptor concentration increases from 10¹³/cm² to 10¹⁸/cm². However,

as the acceptor concentration increases further to $10^{19}/\text{cm}^2$, FF declines a little for higher absorber layer thickness, which may be due to the effect of metallic transition of CTS absorber at this carrier concentration level as described previously. Thickness of absorber layer has minimal effect on FF and remains almost constant for entire thickness variation. Theoretically the maximum value of FF can be achieved as high as 1, however, practically the standard value of FF can vary from 0.7 to 0.85 [6]. In this study, for absorber layer thickness of 2000 nm and carrier concentration of $10^{18}/\text{cm}^2$ shows the highest FF of 0.7, which can be identified as a standard value for thin film solar cell.

Eff of solar cell is the combinational result of V_{oc} , J_{sc} and FF. Acceptor concentration has an incremental effect on J_{sc} , V_{oc} , and FF, which eventually results in increment of Eff up to the acceptor concentration of $10^{18}/\text{cm}^2$. As discussed earlier, due to metallic transition after this critical doping concentration, the value of Eff also sharply drops to a much lower value. On the other hand, thickness of absorber layer shows minimal effect on both V_{oc} and FF; however, it shows moderate incremental effect on J_{sc} . In a word, thickness has a net incremental effect on J_{sc} , V_{oc} and FF, and eventually an incremental effect on Eff, which can be seen from Fig. 2(d). In addition, Eff can be also influenced by interfacial difference of several electronic properties arising from back contact and absorber layer [6]. The difference between back contact metal function and the electron affinity of absorber layer is defined as barrier height for electron (ϕ_{bn}), which has an incremental effect on both J_{sc} and V_{oc} . Since, monoclinic CTS phase has an electron affinity of 4.77 eV and the work function of back metal of Mo is 4.95 eV, therefore the value of ϕ_{bn} is equal to 0.18 eV. The ratio of ϕ_{bn} and band gap (E_g) is an important factor, which determines the maximum efficiency of corresponding solar cell. In this study, the maximum efficiency has been found as 10.86% for a ϕ_{bn}/E_g value of 0.2. This value can be compared with previously reported simulation result for cubic and tetragonal phases. With the same back contact and electron affinity, the cubic and tetragonal phases showed 10% and 8% maximum efficiency for the ϕ_{bn}/E_g ratio of 0.19 and 0.133, respectively [6]. From this analysis, it is evident that the work function of back metal has a large impact on determining the efficiency limit of thin film solar cell. Therefore, further investigation on the effect of back metal work function will be discussed in the subsequent section 3.3.

3.2. Effect of buffer layer thickness and carrier concentration

Buffer layer is a core layer along with absorber layer to form the heterojunction type p-n junction, which is the heart of the CTS based solar cell. In this study, thickness and carrier concentration of CdS buffer layer has been varied from 20 nm to 80 nm and $10^{13}/\text{cm}^2$ to $10^{19}/\text{cm}^2$, respectively. The simultaneous effects of both thickness and carrier concentration of buffer layer on the performance of CTS based solar cell is shown in Fig. 7. The increasing thickness of buffer layer has shown a net decreasing effect on the all performance parameter of CTS solar cell, such as V_{oc} , J_{sc} , FF as well as Eff. This phenomenon can be explained with photon absorption theory, which describes that, any photon having equal or more energy than the band gap can be absorbed by corresponding material. Since, substrate type cell structure (Fig. 1) is taken in this study and the position of buffer layer is situated above the absorber layer from where the light comes in, therefore any photon having wavelength more than 516 nm can be partially absorbed by CdS ($E_g = 2.4$ eV) buffer layer. This absorption rate increases as the thickness of buffer layer increases. Therefore, the number of generated electron-hole pair reduces, which declines the J_{sc} , as can be seen from Fig. 7(b). Moreover, the recombination rate becomes higher in thicker buffer layer due to the lower diffusion length, which results in lower J_{sc} and thus lower efficiency. However, too thin buffer layer is not preferable as this may cause short-circuit in between absorber and TCO through pin-holes [36]. Moreover, a moderate thick buffer layer can serve as a partial protection layer during sputtering of i-ZnO and TCO layers. On the other hand, buffer layer plays an important role to create electric field in the depletion region of solar cell, which essentially controls the separations of generated electron-hole pair. However, too thin buffer layer cannot create the electric field uniformly as can be seen in Fig. 8. The electric field of buffer/absorber interface comes to a stable form only after the buffer layer thickness of 50 nm. Thus 50 nm can be taken as optimum thickness value for buffer layer from this study. Moreover, this value is frequently chosen for buffer layer as reported elsewhere [30].

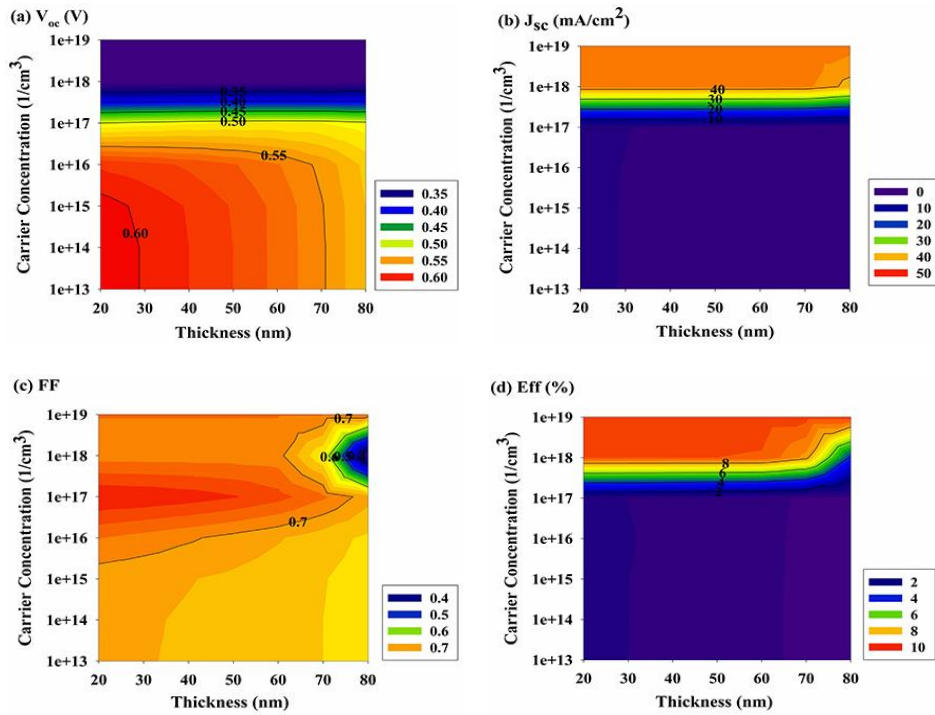


Fig. 7. Concurrent effect of thickness and carrier concentration of absorber layer on the performance of CTS based solar cell.

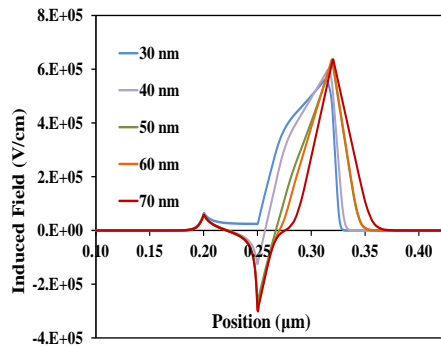


Fig. 8. Effect of buffer layer thickness on the electric field of CTS/CdS interface.

The influence of donor concentration of CdS buffer layer can be also seen in Fig. 7. Since, the acceptor concentration of absorber layer has been taken as the previous optimum value ($10^{18}/\text{cm}^3$), therefore the J_{sc} is found significantly lower (about $2 \text{ mA}/\text{cm}^2$) up to the donor concentration of $10^{17}/\text{cm}^3$. The reason behind this lower J_{sc} and thus lower efficiency has been explained in details in subsection 3.1, where it was concluded that, donor concentration should not be lower than acceptor concentration as it cause serious recombination in the buffer/absorber interface. As the donor concentration equal to the value of acceptor concentration, the electron traps for recombination decreases to a much lower level at the buffer/absorber interface, which ultimately sharply increases the J_{sc} and resulted in massive increment in Eff. As the donor concentration increased further to $10^{19}/\text{cm}^3$, a moderate increment of J_{sc} and Eff can be seen in Fig. 7, which ensures further decrement of electron trap in the absorber/buffer interface. However, beyond the doping level of $10^{18}/\text{cm}^3$ is not a good choice for a semiconductive material, as it can be turned into metallic regime due to ‘Mott transition’ rule as described earlier. Therefore, in this study, donor concentration of $10^{18}/\text{cm}^3$ can be taken as optimum value for CdS buffer layer.

3.3. Effect of back metal work function

To evaluate the influence of the work function of back contact metal, it is varied from 4.8 to 5.6 eV in this study. During this time the thickness and acceptor concentration of absorber layer are kept 2000 nm and $10^{18}/\text{cm}^3$, respectively while the thickness and donor concentration of buffer layer are kept 50 nm, and $10^{18}/\text{cm}^3$, respectively. The temperature is maintained at 300^0 K and other parameter values remained constant. Table 3 summarizes the variation in V_{oc} , J_{sc} , FF, and Eff of CTS solar cell for different back metal which has the work function ranging from 4.8 eV to 5.6 eV, such as osmium (Os), zinc (Zn), molybdenum (Mo), cobalt (Co), tungsten (W), nickel (Ni), gold (Au), and palladium (Pd). Here, the work function of different metals is taken from the work reported by Michaelson et al. [39]. Moreover, Fig. 9 illustrates the effect of back contacts on the output characteristics of CTS solar cell by increasing the work function of back metal from 4.8 eV to 5.6 eV with a step of 0.1 eV. The lower range of tested back metal work function is selected as 4.8 eV, since the Schottky barrier height for hole is too high before this value which leads convergence failure during the simulation, while the upper range is taken as 5.6 eV, because the Schottky barrier height becomes negative after this value, which is not a reasonable operating condition.

Table 3. Summary of output parameters of CTS solar cell for different back contact metals.

Back contact metal	Work function (eV)	V_{oc} (V)	J_{sc} (mA/cm^2)	FF	Eff (%)	CTE ($10^{-6}/\text{K}$)
Os	4.84	0.2	43.237	0.628	5.436	2.2 - 6.1
Zn	4.90	0.26	43.281	0.682	7.679	15
Mo	4.95	0.31	43.310	0.715	9.610	4.8 - 5.1
Co	5.00	0.36	43.338	0.742	11.576	12 - 14
W	5.25	0.51	43.452	0.798	17.870	4.5 - 4.6
Ni	5.35	0.51	43.491	0.798	17.918	13
Au	5.47	0.51	43.541	0.798	17.944	14
Pd	5.60	0.51	43.620	0.798	17.987	11 - 12

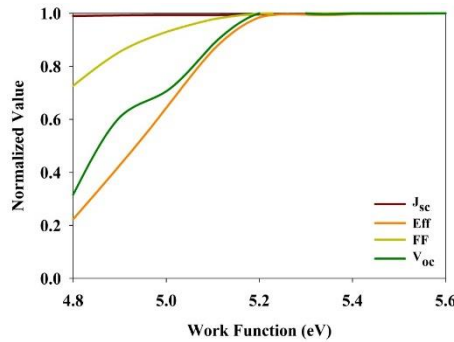


Fig. 9. Effect of back metal work function on the normalized output parameters of monoclinic CTS solar cell.

It is observed from Fig. 9 that there is a considerable improvement in solar cell parameters due to increasing work function of the back metal contact. The V_{oc} and FF show sharp increment gradient as the work function changes from 4.8 to 5.2 eV, which resulted in massive raise of Eff. The increment of V_{oc} due to back metal work function raise can be attributed to the reduction of Schottky barrier height for hole (ϕ_{bp}). The ϕ_{bp} is inversely proportional to the work function of back contact metal [6]. Therefore, as the work function of back metal increases, the ϕ_{bp} of metal semiconductor junction decreases, and eventually the interfacial recombination reduces. As a

result, V_{oc} improves, and this increased V_{oc} leads to FF raise according to equation (6), while J_{sc} remains almost constant during the entire range of work function. The increment of both V_{oc} and FF results in Eff increment as can be seen in Fig. 9. However, as the value of back metal work function crosses 5.2 eV, V_{oc} and FF become almost constant up to the end. Therefore, it can be assumed that saturation of back metal work function has been attained after 5.2 eV and any back metal having work function larger than this saturation value can be taken as optimum metal as back contact for monoclinic phase CTS solar cell. On the other hand, the coefficient of linear thermal extension (CTE) is an important parameter which should be given priority in terms of mechanical stability [5], and this value should be lower for a perfect back contact. The CTE of corresponding back metals mentioned in table 3 have been taken from the Ref. [40]. From the table 3, it can be seen that Os, Mo and W are the only three metals that has CTE value lower than 10. However, only Mo is reported as the back contact metal in all the practical CTS solar cell [8, 15, 41, 42]. From the analysis discussed above it can be decided that Mo is not the optimum back contact for CTS based solar cell. According to the saturation point of back metal as seen from Fig. 9 and the CTE value mentioned in table 3, it can be concluded that, W can be regarded as the optimum back metal for monoclinic phase CTS solar cell. The band alignment of optimized back metal (W) semiconductor (CTS) interface has been shown in Fig. 10.

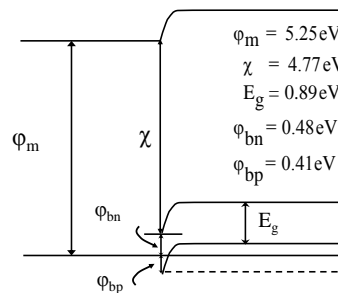


Fig. 10. Metal-semiconductor junction band alignment optimized back metal (W) and monoclinic phase CTS absorber.

3.4. Effect of operating temperature

Operating temperature plays a crucial role for the output performance of solar cells. Usually, solar panels are installed at the outdoor condition, where standard operating temperature (300 °K) may not be maintained all time. Therefore, the effect of operating temperature should be understood properly to maintain the tolerance at minimum level. In this study, the operating temperature has been varied from 300 °K to 400 °K with a step of 20 °K and the effect of temperature variation on V_{oc} , J_{sc} , FF and Eff of monoclinic phase CTS solar cell has been illustrated in Fig. 11. During this time, all the variable parameters of CTS have been taken as previous obtained optimized value.

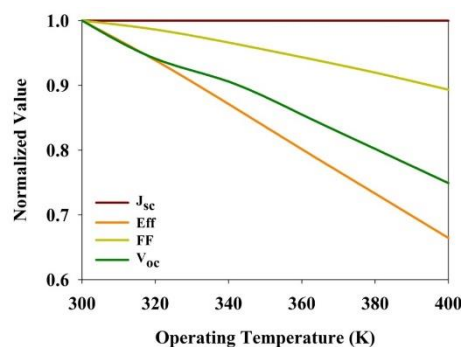


Fig. 11. Effect of operating temperature on the output performance on the monoclinic phase CTS solar cell.

From the Fig. 11, it is observed that, V_{oc} and FF linearly decreased with increasing temperature, while J_{sc} remains almost constant through the entire temperature range. The reason behind this phenomenon is the temperature dependence of reverse saturation current [38, 43]. As the operating temperature increases, the reverse saturation current is increased, which ultimately decreased V_{oc} according to equation 2. On the other hand, increased temperature causes more electron-hole pair due to additional thermal energy. However, recombination rate of electron also increased behind the depletion region due to unstable situation. Therefore, J_{sc} remains almost constant during the entire temperature variation. As a result, Eff declines linearly with a temperature coefficient of $-0.33\%/K$, which is a reasonable value of solar cell for outdoor installation.

3.5. Optimized monoclinic phase CTS thin film solar cell characteristics

Fig. 12 is shown the comparison between J-V characteristics of before and after optimization of monoclinic phase CTS solar cell. From the figure it can be observed that, optimized CTS solar cell exhibits much better performance. The optimized CTS solar cell delivers as high as 17.87% power conversion efficiency while before optimization this cell delivers only 4.83% efficiency. Actually, the increased efficiency of optimized CTS solar cell primarily comes from the improvement of V_{oc} , which shows a massive improvement from 185 mV to 516 mV after the optimization. Optimized back metal work function mainly attributed to the improvement of V_{oc} . FF also shows a moderate improvement from 0.619 to 0.798 during this optimization study. Along with output parameters the QE of optimized CTS solar also shows a decent improvement, which is shown in Fig. 13. The improvement of QE can be attributed to the optimized thickness of both buffer and absorber layer as well as the optimized carrier concentration of these two layers. The power conversion efficiency of optimized CTS solar cell (17.87%) is acceptable for commercial production and further analysis is needed to reach the Shockley-Queasier limit, which is around 30% for of a single junction CTS solar cell [44].

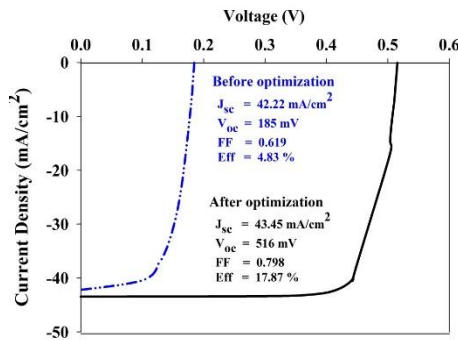


Fig. 12. Comparison of J-V characteristics of before and after optimized monoclinic CTS solar cell.

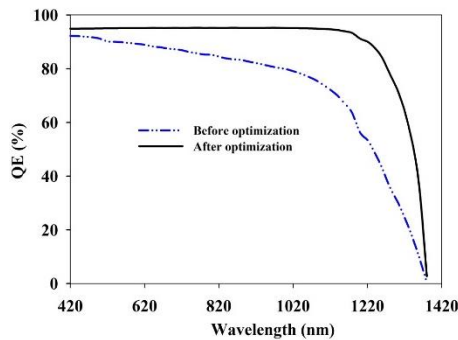


Fig. 13. Comparison of QE of before and after optimized monoclinic CTS solar cell.

4. Conclusions

In this study, baseline SLG/Mo/CTS/CdS/ZnO solar cell has been taken to optimize thickness and carrier concentration of both absorber and buffer layer. The optimization procedure has carried out with the aid of output performance parameters such as V_{oc} , J_{sc} , FF, and Eff. In some special cases, QE, depletion width, electrical field analysis are also carried out to seek out the pin point of optimization. For monoclinic absorber layer, optimum thickness and carrier concentration were found to be 2000 nm and $10^{18}/\text{cm}^3$, respectively. The thickness of buffer showed a decline effect on the cell performance. However, too thin buffer layer is not preferable due to leakage current probability. Therefore, a 50 nm thick buffer layer with a carrier concentration of $10^{18}/\text{cm}^3$ was chosen as optimized value. Optimization of absorber and buffer layer parameters were carried out with back contact of Mo, and showed 9.61% efficiency for the best CTS cell. However, a massive improvement was observed during the optimization of back metal work function.

The efficiency was increased linearly up to the work function of 5.20 eV, then, it saturated and remained almost constant to the end. Since, there is no back contact having this work function, therefore, W ($\phi_m = 5.25$ eV) was chosen as the optimum back metal, which has a minimum level of CTE also. Using W as a back contact, the power conversion efficiency was reached as high as 17.87%, which was beyond the commercial benchmark level. The effect of operating temperature was also tested in this study and found a gradual decline with temperature with a rate of $-0.33\%/K$. This decline rate is an indicator that CTS solar cell is fit for outdoor installation. All the analysis done above showed that monoclinic CTS solar cell can be taken as upcoming next generation solar cell. However, further research is needed to improve V_{oc} of this cell to achieve the Shockley-Queasier limit.

Acknowledgments

All the findings achieved in this study are the responsibility of the authors. The authors would like to acknowledge and appreciate UGC and DUET for the contribution of research grant.

References

- [1] M. A. Green, Y. Hishikawa, E. D. Dunlop, H. L. Dean, J. Hohl-Ebinger, A. W. Y. Ho-Baillie, *Progress in Photovoltaics: Research and Applications* **27**(1), 565 (2019).
- [2] B. A. Andersson, *Progress in Photovoltaics: Research and Applications* **8**(1), 61 (2000).
- [3] B.-A. Schubert, I. M. Kotschau, S. Cinque, H.-W. Schock, *Proceedings of the 23rd EU-PVSEC, Valencia*, 3788 (2008).
- [4] W. Wang, M. T. Winkler, O. Gunawan, T. Gokmen, T. K. Todorov, Y. Zhu, D. B. Mitzi, *Advance Energy Materials* **4**(7), 1301465 (2014).
- [5] M. Patel, A. Ray, *Physica B Condensed Matter* **407**, 4391 (2012).
- [6] E. S. Hossain, P. Chelvanathan, S. A. Shahahmadi, K. Sopian, B. Baisa, N. Amin, *Current Applied Physics* **18**(1), 79 (2018).
- [7] S. Chen, A. Walsh, X. G. Gong, S. H. Wei, *Advance Materials* **25**(11), 1522 (2013).
- [8] R. Chierchia, F. Pigna, M. Valentini, C. Malerba, E. Salza, P. Mangiapane, T. Polichetti, A. Mittiga, *Physica Status Solidi C* **13**(1), 35 (2016).
- [9] S. Sato, H. Sumi, G. Shi, M. Sugiyama, *Physica Status Solidi C* **12**(6), 757 (2015).
- [10] T. A. Kuku, O. A. Fakolujo, *Solar Energy Materials*, **16**(1), 199 (1987).
- [11] P. Fernandes, P. Salome, A. D. Cunha, *Journal of Physics D: Applied Physics* **43**(21), 215403 (2010).
- [12] S. Chen, J.-H. Yang, X.-G. Gong, A. Walsh, S.-H. Wei, *Physical Review B* **81**(24), 245204 (2010).
- [13] T. A. Kuku, O. A. Fakolujo, *Sol. Energy Mater.* **16**, 199 (1987).
- [14] M. Nakashima, J. Fujimoto, T. Yamaguchi, M. Izaki, *Applied Physics Express* **8**(4), 042303 (2015).

- [15] M. Umehara, Y. Takeda, T. Motohiro, T. Sakai, H. Awano, R. Maekawa, *Applied Physics Express* **6**(4), 045501 (2013).
- [16] D. Avellaneda, M. Nair, P. Nair, *Journal of the Electrochemical Society* **157**(6), D346 (2010).
- [17] C. Wu, Z. Hu, C. Wang, H. Sheng, J. Yang, Y. Xie, *Applied Physics Letters* **91**(14), 143104 (2007).
- [18] Y.-T. Zhai, S. Chen, J.-H. Yang, H.-J. Xiang, X.-G. Gong, A. Walsh, J. Kang, S.-H. Wei, *Physical Review B* **84**(7), 075213 (2011).
- [19] Z. Tang, K. Kosaka, H. Uegaki, J. Chantana, Y. Nukui, D. Hironiwa, T. Minemoto, *Physica Status Solidi A* **212**(10), 2289 (2015).
- [20] A. Kanai, H. Araki, A. Takeuchi, H. Katagir, *Physica Status Solidi B* **252**(6), 1239 (2015).
- [21] H. Zhu, A. K. Kalkan, J. Hou, S. J. Fonash, M. Al-Jassim, Applications of AMPS-1D for solar cell simulation, in: *AIP Conference Proceedings*, AIP, 309 (1999).
- [22] F. Liu, J. Zhu, J. Wei, Y. Li, M. Lv, S. Yang, B. Zhang, J. Yao, S. Dai, *Applied Physics Letters* **104**(25), 253508 (2014).
- [23] P. J. McElheny, J. K. Arch, H.-S. Lin, S. J. Fonash, *Journal Applied Physics*, **64**, 1254 (1988)
- [24] S. Fonash, J. Arch, J. Cuiffi, J. Hou, W. Howland, P. McElheny, A. Moquin, M. Rogosky, T. Tran, H. Zhu, The Pennsylvania State University, USA, 1997.
- [25] P. Jackson, R. Wuerz, D. Hariskos, E. Lotter, W. Witte, M. Powalla, *Physical Status Solidi RRL* **10**(8), 583 (2016).
- [26] J. H. N. Tchognia, Y. Arba, K. Dakhsi, B. Hartiti, A. Ridah, 3rd International Renewable and Sustainable Energy Conference (IRSEC), 15936890 (2015).
- [27] M. Gloeckler, A. Fahrenbruch, J. Sites, *Proceedings of 3rd World Conference on Photovoltaic Energy Conversion*, 2003, IEEE, 491 (2003).
- [28] U. Chalapathi, Y. Jayasree, S. Uthanna, V. Sundara Raja, *Vacuum* **117**, 121 (2015).
- [29] R. Bodeux, J. Leguay, S. Delbos, *Thin Solid Films* **582**, 229 (2015).
- [30] E. S. Hossain, P. Chelvanathan, S. A. Shahahmadi, B. Bais, M. Akhtaruzzamanb, S. K. Tiong, K. Sopian, N. Amin, *Solar Energy* **177**, 262 (2019).
- [31] E. S. Hossain, P. Chelvanathan, S. A. Shahahmadi, M. T. Ferdaous, B. Bais, S. K. Tiong, N. Amin, *Chalcogenide Letters* **15**(10), 499 (2018).
- [32] A. Niemegeers, M. Burgelman, A. De Vos, On the CdS/CuInSe 2 conduction band discontinuity, *Applied Physics Letters* **67**(6), 843 (1995).
- [33] S. S. Li, p-n junction diodes, in: S.S. Li (Ed.), *Semiconductor Physical Electronics*, Springer New York, New York, NY, 334 (2006).
- [34] M. A. Green, *Solar Cells: Operating Principles, Technology, and System Applications*, Prentice-Hall, Inc., Englewood Cliffs, NJ, 1982.
- [35] N. Mott, *Review Modern Physics* **40**(4), 677 (1968).
- [36] M. Patel, A. Ray, *Physica B: Condense of Matter* **407**(21), 4391 (2012).
- [37] M. A. Green, *Solid-State Electron*, **24**(8), 788 (1981).
- [38] K. Sobayel, K. S. Rahman, B. M. R. Karim, M. O. Aijaz, M. A. Dar, M. A. Shar, H. Misran, N. Amin, *Chalcogenide Letters* **15**(6), 307 (2018).
- [39] H. B. Michaelson, *Journal Applied Physics* **48**(11), 4729 (1977).
- [40] ASM International, *ASM ready reference: thermal properties of metals, thermal expansion*, 2011 (Chapter 2). http://www.owl.net.rice.edu/_msci301/ThermalExpansion.pdf, (accessed 06.25.11).
- [41] Y. Dong, J. He, L. Sun, Y. Chen, P. Yang, J. Chu, *Material Science in Semiconductor Process* **38**,171 (2015).
- [42] N. Aihara, A. Kanai, K. Kimura, M. Yamada, K. Toyonaga, H. Araki, A. Takeuchi, H. Katagiri, *Japanese Journal of Applied Physic*, **53**, 05FW13 (2014).
- [43] P. Lin, L. Lin, J. Yu, S. Cheng, P. Lu, Q. Zheng, *Journal of Applied Science and Engineering* **17**(4), 383 (2014).
- [44] S. A. Vanalakar, G. L. Agawane, A. S. Kamble, C. W. Hong, P. S. Patil, J. H. Kim, *Solar Energy Materials & Solar Cells* **138**, 1 (2015).